SCOPE | SAUDI INTERNATIONAL CONFERENCE ON NUCLEAR POWER ENGINEERING

Proceedings of SCOPE
13-15 Nov. 2023 – KFUPM
Paper 23155

Large Eddy Simulation of a Simplified Pressurized Thermal Shock Scenario

Algazlan, Osamah[1], Alruwaished, Abdulaziz[1], Alsafi, Osama[1], Aljohani, Mohammed[1], Aldoughan, Abdulrahman[1], Almalki, Abdullah[1] Shams, Afaque[1,2], Kwiatkowski, Tomasz[3]*

[1]King Fahad University of Petroleum & Minerals (KFUPM), Saudi Arabia
[2]Interdisciplinary Research Center for Renewable Energy and Power Systems (IRC-REPS), KFUPM, Saudi Arabia
[3]National Centre for Nuclear Research (NCBJ), Poland

*Corresponding author: s201815300@kfupm.edu.sa *(O. Algazlan).*

Abstract – The Reactor Pressure Vessel (RPV) is a crucial component in nuclear systems. One of the mechanisms that can jeopardize the integrity of RPV is a transient condition called Pressurized Thermal Shock (PTS). During accidents such as Loss of Coolant Accidents (LOCA), emergency systems are initiated to mitigate the accident. The cold water injected by the Emergency Core Cooling System (ECCS) causes a quick cooling of the downcomer and internal surface of the RPV. As a result of this rapid cooling, large temperature gradients and thermal stresses occur, which represents the PTS phenomenon. These issues cannot be accurately predicted through experimental means, nor through one dimensional thermal hydraulic system codes. However, they can be predicted through the proper use of numerical methods such as Computational Fluid Dynamics (CFD) to simulate the thermal hydraulics of the Reactor Coolant System (RCS). This has been done before through a direct numerical simulation. Nevertheless, this simulation is done using a low Reynolds number. However, such a high a fidelity simulation can act as benchmark for a Large Eddy Simulation to verify the methodology. Our primary focus encompasses two regions: the square duct and the downcomer. Preliminary results indicate strong resemblance between LES and DNS data, in terms of velocity and temperature contours in both regions. This agreement emphasizes the potential of LES, when applied rigorously, to not only match the benchmark DNS but also extend its capabilities to higher Reynolds numbers, thereby providing a more comprehensive understanding of the flow dynamics in such critical scenarios.

Keywords: Thermal Hydraulics, Pressurized thermal shock, Simulation.

I. Introduction

There are several mechanisms that can reduce the life expectancy of a Nuclear Power Plant (NPP) components, and ultimately reduce the NPP lifetime and pose safety risks. The Reactor Pressure Vessel (RPV) is a crucial component in nuclear systems; hence it undergoes periodical analysis during its lifetime to check its integrity [1]. One of the mechanisms that can jeopardize the integrity of RPV is a transient condition called Pressurized Thermal Shock (PTS). During accidents such as Loss of Coolant Accidents (LOCA), emergency systems are initiated to mitigate the accident. The cold water injected by the Emergency Core Cooling System (ECCS) causes a quick cooling of the downcomer and internal surface of the RPV. As a result of this rapid cooling, large temperature gradients and thermal stresses occur, which represents the PTS phenomenon. Consequently, defects in the embrittled RPV, which can exist due to neutron irradiation, can propagate within the vessel walls. In the meantime, the pressure is either maintained or increased a little bit. These issues can be predicted through the proper use of numerical methods to simulate the thermal hydraulics of the Reactor Coolant System (RCS).

In nuclear thermal hydraulics, two categories of simulations can be specified, system codes and three-dimensional numerical simulations. System codes are based on one-dimensional equations that simplify flow analysis, where complex three-dimensional flows cannot be studied. On the other hand, advanced numerical simulations can represent three-dimensional complex flows, which are encountered during PTS. Direct numerical simulation (DNS) is ideal as it provides the most accurate numerical results; however, it requires very large computational resources, which makes it less practical for most of the industrial applications. On the contrary, Reynolds-Averaged Navier-Stokes (RANS) turbulence modelling approach requires less computational resources. Therefore, making it a widely used industrial tool. Nevertheless, the application of RANS methodology for any industrial scenario, such as the PTS case, requires a proper validation. In between, DNS and RANS, there exist an approach called the Large Eddy Simulation (LES) which

proves to be the most suitable modelling approach for studying the PTS scenario; it is less expensive than DNS and yet it provides accurate results. Previous work has been done to simulate PTS utilizing the LES turbulence model as found in [2], where a transient single-phase TOPFLOW test case was used to validate the simulation. Following this work, Shams et al. [3] designed a simplified PTS configuration with the use of DNS. The effect of crossflow velocity on flow and heat transfer characteristics of the impinging jet was considered in [4], where Re=13400 was used. In [5], the LES of an impinging jet was performed in a heated, crossflow wall-mounted cube and a Re=5341 was used.

In 2018, a Quasi-DNS (q-DNS) numerical simulation was conducted by Shams & Komen [6] for a simplified single-phase flow PTS case (for more details, see section 2). This q-DNS was later used, by Shams et al. [3], as initial conditions to perform a high-quality reference DNS study. This paper adopts the exact simplified PTS case studied by Shams et al [7], in which the cold leg is considered as square rather than a round pipe. Thus, injects a square jet with the Re=5400, and the distance to the core barrel is 0.4865 times the jet width. Furthermore, constant fluid properties are considered. Accordingly, to mimic the buoyance effects (similar to the real-life scenario) as the cold jet interacts with the hot core barrel, transverse-flow from the top is utilized to force the jet to flow downward, with a velocity ratio of 10. Since the jet has a square profile, the flow fields at the downcomer are non-homogeneous, which resembles a more realistic flow behaviour compared to round jets, at the expense of higher computational cost. Additionally, two boundary conditions (isothermal and adiabatic) are imposed at the downcomer walls to study the heat transfer phenomenon. The isothermal boundary condition represents the initial stage, where the temperature gradients near the wall are developing to reach high values. In contrast, the adiabatic boundary condition resembles the steady-state behaviour of the phenomenon, where negligible temperature gradients exist near the walls. However, although DNS studies are accurate, the inherent high computational cost associated with such studies renders it unfeasible for most industrial applications. The present paper investigates the flow fields and thermal behaviour of the PTS case using the LES turbulence model. Using DNS results for benchmarking, to assess the prediction capabilities of the LES outcomes. The LES method can study PTS at higher Reynolds numbers, bringing simulations closer to real-world conditions. Ultimately, the aim is to simulate PTS with LES at these higher Reynolds numbers. This will facilitate the creation of a validation database for refining and validating RANS-based models, pushing the prediction of PTS closer to industrial applicability. The rest of the article is organized as follows: In section II, the adopted numerical methodology including flow parameters, boundary conditions, meshing and turbulence modelling is given; section III discusses the obtained results, and accordingly they are summarized in section IV.

II. NUMERICAL METHODOLOGY

A. Flow Configuration

The PTS configuration used in this paper is similar to the one used by Shams et al. [3] and it is depicted in Figure 1. In this geometric configuration, a square cold leg intersects a planar downcomer of the RPV perpendicularly. For the cold leg, a square configuration is used with D_c = 0.15 m and length L = 10.15D_c. Taking the origin to be at the centre of the interface between the cold leg and the downcomer, the dimensions of the downcomer are as follow: the upper height H_1 = 10D_c, the lower height H_2 = 23.3D_c, the thickness of the downcomer D_d = 0.4865D_c, and the half width W = 10D_c. There are two inlets, inlet 1 and inlet 2. Inlet 1 is in the duct perpendicular to the downcomer, whereas the Inlet 2 is from the top of the downcomer.

B. Flow Parameters and Boundary Conditions

Reynolds number in the bulk of the fluid is chosen to be $Re = \frac{U_c D_c}{\nu} = 5400$, where ν is the constant fluid kinematic viscosity. It corresponds to an average friction Reynolds number $Re_\tau = 180$ in the cold leg, with $Re_\tau = u_\tau h_c/\nu$, where $u_\tau = \sqrt{\tau_w/\rho}$ is the friction velocity, with τ_w the temporal and spatial averaged wall shear stress computed in the duct, and ρ is the constant fluid density. Finally, the Prandtl number is set as $Pr = \nu\alpha = 1$, where α is the constant thermal diffusivity of the fluid.

The bulk velocity U_c = 0.36 and fluid temperature T_c = 293 K are imposed in the cold leg. Recycling the velocity field in the first half of the duct with a length of 6.6D_c forces a fully developed turbulent velocity profile in the cold leg. On the secondary inlet at the top of the downcomer, a constant velocity U_2 = 0.1U_c and a constant hot fluid temperature T_h = 353 K are imposed on the surface with uniform profiles. The downcomer's vessel and barrel walls are either adiabatic or isothermal and are no-slip walls. The two side walls that encompass the downcomer in the horizontal direction are adiabatic no-slip walls. Finally, it is assumed that the downcomer's bottom surface acts as an outlet boundary.

C. Meshing Strategy

Structured hexahedral mesh was generated for the computational domain, which consists of the square duct and the downcomer. The meshing capabilities of the commercial software STAR-CCM+ version 2210 were utilized, which provides a wide range of features that facilitated the meshing process. The domain was subdivided into two regions, namely the square-duct and the downcomer. This permit manipulating the mesh easily to account for the flow physics in different regions, as shown in Figure 2.

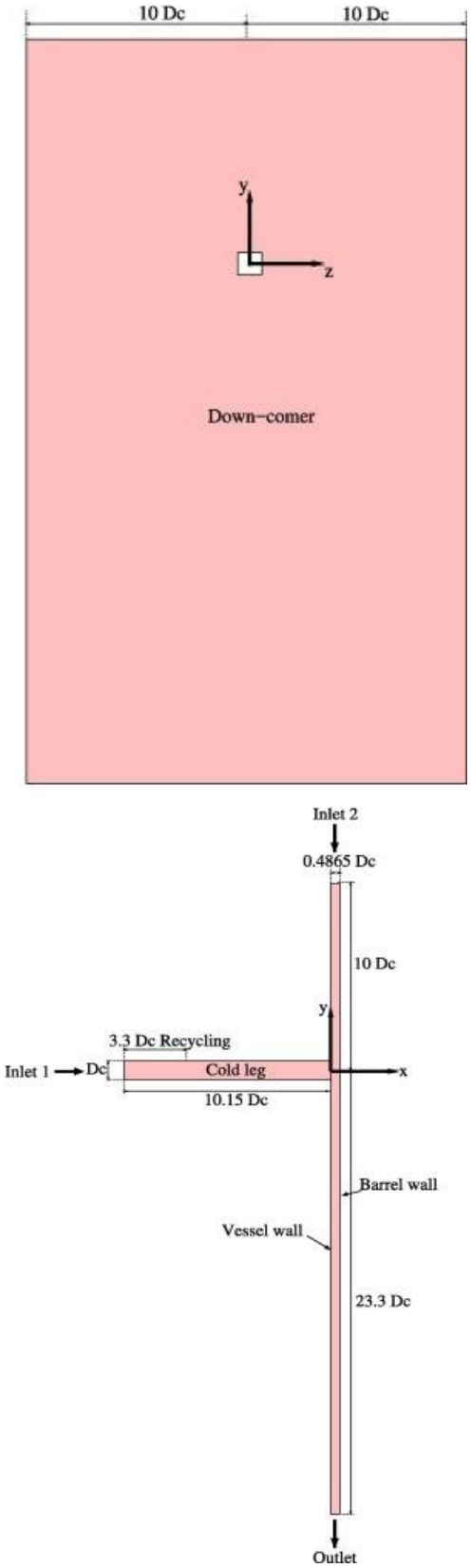

Figure 1. Sketch of the PTS geometry to be used (adopted from Shams et al. [3]).

Additionally, special care was devoted to the near-wall cells in each region, as to capture the large flow gradients. Following the q-DNS study of Shams et al. [6] the LES meshing is performed, and the final meshing parameters are: the first cell $y^+ = 0.5$; $(\Delta y^+ = \Delta z^+) < 10$, $\Delta x^+ < 15$. Here, the non-dimensionalized cell size, such as y^+ is computed by using:

$$y^+ = \frac{u_\tau y}{\nu}$$

By taking in account these meshing parameters, the overall mesh for this PTS geometry consists of ~ 20 million grid points, making it a very fine mesh to perform the LES study. Figure 3 shows a representative cross-sectional view of the square-duct mesh. The cell skewness was controlled by imposing limits on the boundary layer non-dimensional quantities.

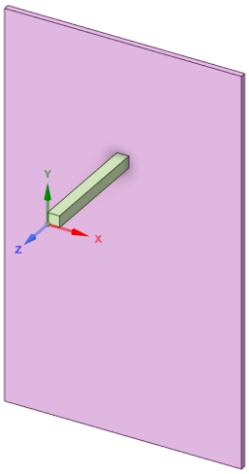

Figure 2. Trimetric view of the subdivided computational domain.

III. NUMERICAL SCHEMES

The current simulation is run using the commercially available finite volume code STAR-CCM+ (STAR-CCM+, 2022). For this flow configuration, it was found that applying a purely central scheme causes numerical instabilities, therefore, for spatial discretization, a second order central scheme with 5% boundedness (of a second order upwind scheme) has been used. This is also consistent with the pioneering work of Shams et al. [8]. Additionally, the temporal discretization is done using a second order implicit scheme. The pressure-velocity coupling of the Rhie-and-Chow type is used in combination with a SIMPLE-type algorithm to perform the current discretization. The details of the scheme are available in the code manual (STAR-CCM+, 2022).

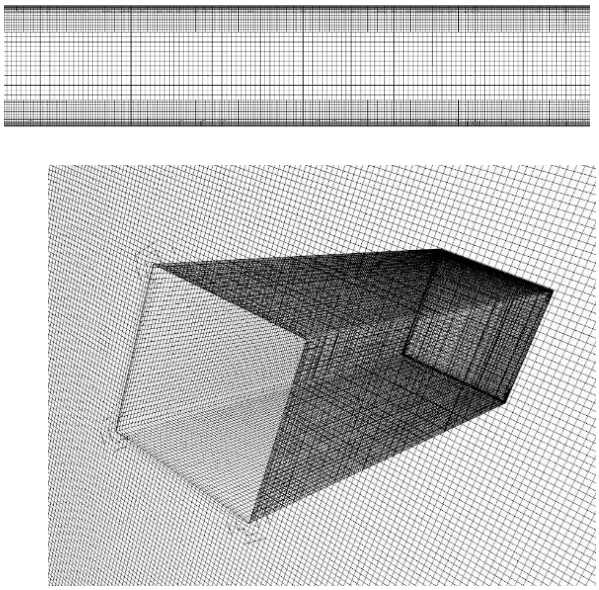

Figure 3. Representative view of the mesh in square duct.

IV. TURBULENCE MODELING

In this study, an LES has been performed to investigate the flow in the aforementioned domain. What separates LES from the other turbulence models is the ability to solve the Navier-Stokes equations for the larger eddies and model the smaller eddies mathematically. The large eddies refer to those larger than the grid size, which depend on how fine the mesh is. On the other hand, the smaller eddies are the sub-grid scale eddies (SGS), which are assumed isotropic to simplify the modelling approach. To solve the Navier-Stokes equations, a filter is used to obtain the SGS stresses, which are represented by the turbulent stress tensor (τij) as:

$$\tau_{ij} - \frac{1}{3}\tau_{kk}\delta_{ij} = -2\mu_t \bar{S}_{ij}$$

Here, μ_t is the SGS turbulent viscosity and S_{ij} is the strain rate tensor. To model the SGS viscosity, a Wall Adapting Local-Eddy viscosity (WALE) model is utilized, which was proposed by Nicoud and Ducros [9]. It is constructed to correct the behaviour of the SGS viscosity as it approaches the wall. This correction is done through squaring the velocity gradient tensor which accounts for both the strain and rotation rates to obtain the local-eddy viscosity. No matter if the mesh is structured or not, this model works well with both, since no dynamic procedure or explicit filtering is used. Other modelling approaches were considered such as the Lily-Smagorinsky or the Van Driest damping, yet these do not produce favourable results for wall bounded flows. Additionally, WALE produces fewer grid induced problems, and shows a y^3 behaviour of the SGS viscosity as the flow approaches the wall. Finally, since it relies on both the strain and rotation rates, it can perform exceptionally well for this study. The parameters to model the eddy viscosity using WALE are:

$$\mu_t = \rho L_S^2 \frac{\left(S_{ij}^d S_{ij}^d\right)^{\frac{3}{2}}}{\left(S_{ij}^d S_{ij}^d\right)^{\frac{5}{2}} + \left(S_{ij}^d S_{ij}^d\right)^{\frac{5}{4}}}$$

$$S_{ij}^d = \frac{1}{2}\left(\bar{g}_{ij}^2 - \bar{g}_{ji}^2\right) - \frac{1}{2}\delta_{ij}\bar{g}_{kk}^2$$

$$\bar{g}_{ij} = \frac{\partial \bar{u}_i}{\partial x_j}$$

$$L_s = C_{\omega} V^{\frac{1}{3}} \quad \text{where,} \quad C_{\omega} = 0.544$$

$$S_{ij}^d S_{ij}^d = \frac{1}{6}(S^2 S^2 + \Omega^2 \Omega^2) + \frac{2}{3}S^2\Omega^2 + 2IV_{S\Omega}$$

V. RESULTS AND DISCUSSION

It is worth mentioning that the main purpose of the current LES computation is to assess its capability in reproducing the complex three-dimensional PTS scenario. In this regard, the available DNS [3] is considered as a reference. For simplicity, the obtained results are compared in two parts, i.e. (A) The square duct, and (B) the downcomer.

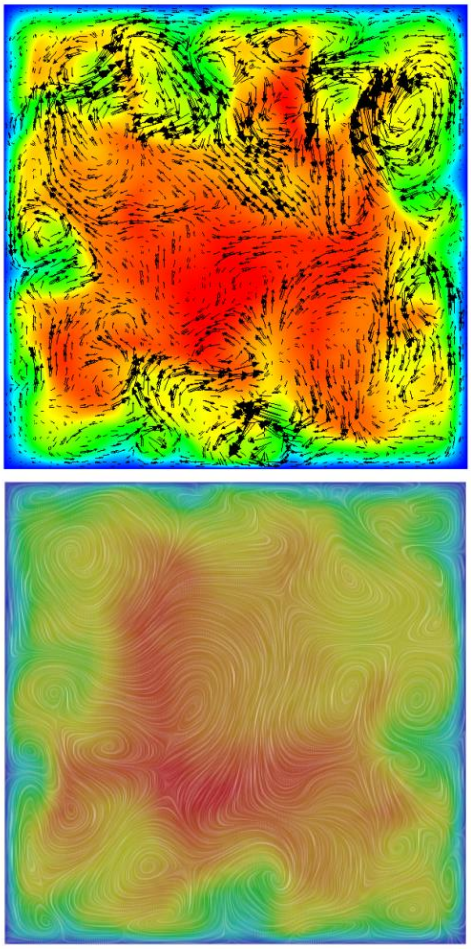

Figure 4. Iso-contours of velocity at the mid cross-section of the duct field (Top) DNS (Bottom) LES

A. The Square Duct

Flow in a square duct exhibits non-linear behavior and is much more complex than a simple (circular) pipe flow. In Figure 4, the velocity contours at the mid cross-section of the duct are shown for LES and the reference DNS case. It can be seen that the flow is highly turbulent and fully developed. It exhibits more complex three-dimensional flow regime with systematic recirculation regions covering the whole duct. The interaction of these recirculation regions gives rise to secondary recirculation regions at each corner of the duct. As a consequence, the flow regime is highly non-linear; hence, making it more challenging for low-order turbulence modelling approaches to predict it correctly. Furthermore, this obtained velocity field has been compared with the reference DNS and is shown as a plot in Figure 5 where the profile is taken from the wall to the center of the duct. It is worth noticing that the LES results are in very good agreement with the reference DNS data.

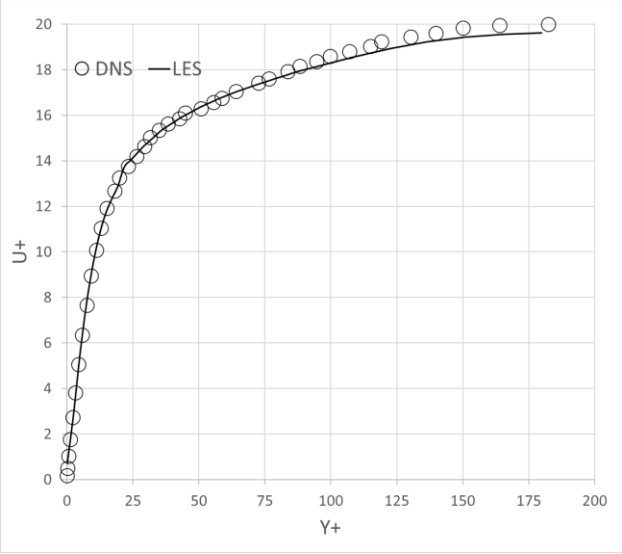

Figure 5. Comparison of velocity profile in the duct from the wall to the middle.

B. The Downcomer

The fully developed turbulent flow from the duct hits the barrel wall. Accordingly, the flow field has a stagnation region, and it evolves into a more complex flow and temperature fields, as depicted in Figure 6. Additionally, 5 regions (indicated by the small box in Figure 6) of the flow leaving the duct are of special interest, in which it causes the formation of vortices due to the impinging nature of the flow. In region 1, the flow coming from the top of the duct hits the barrel wall and is deflected upwards, only to be brought downward by the flow from the second inlet. This interaction creates a recirculation region. In region 2, the flow leaving from the side of duct is deflected horizontally and is then brought downward by the flow from above. Furthermore, the flow from region 4 is deflected in the radial direction and thus breaks the aforementioned recirculation region into two more vortices. Moreover, the flow from region 3 is deflected downward along the downcomer. Finally, the flow from region 5 is deflected radially in the downward direction, notably the flow from this region possesses much lower velocities compared to surrounding regions due to the pressure suction effect. Following the impingement region, the turbulent duct flow breaks into small turbulent scales as highlighted by the iso-surfaces of Q-criterion in Figure 7.

These small structures undergo large shear stresses in the flow and eventually leads to the overall mixing in the downcomer. These results are consistent with the reference DNS data (for more details readers are referred to [3]). Figures 8 and 9 illustrate the instantaneous velocity and thermal fields (obtained from the adiabatic boundary condition) at the mid cross-section of the downcomer. For better understanding, these results are compared with the DNS computations. Looking at Figure 8, it is clearly noticeable that the overall turbulence flow behaviour is nicely captured by the current LES study. This highlights the supremacy of the LES method over the low-order turbulence modelling approaches to correctly predict the complex flow regimes.

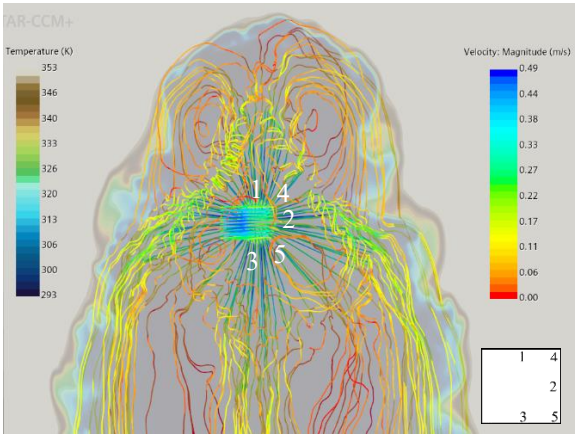

Figure 6. Evolution of streamlines from duct, at the impinging region, and in the downcomer (Box: duct regions mentioned above) .

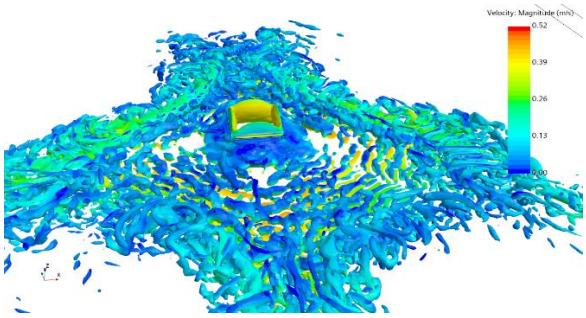

Figure 7 Iso-surfaces of Q-criterion colored with velocity field.

In Figure 9, a qualitative comparison of the temperature field is given. Since the current LES has yet to reach statistical convergence, the instantaneous temperature field has been compared with the mean temperature field of the reference DNS. Once again, it is clear that the overall thermal field has been nicely predicted by the LES. This also validates the fact that once the LES provides a better agreement in comparison with the DNS, it has the potential to serve as a reference database if properly performed at a higher Reynold number for such complex flow regime. It is worth mentioning that the current LES simulation is still in progress and will soon yield statistical convergence of flow and thermal fields. Accordingly, they will be presented at the conference.

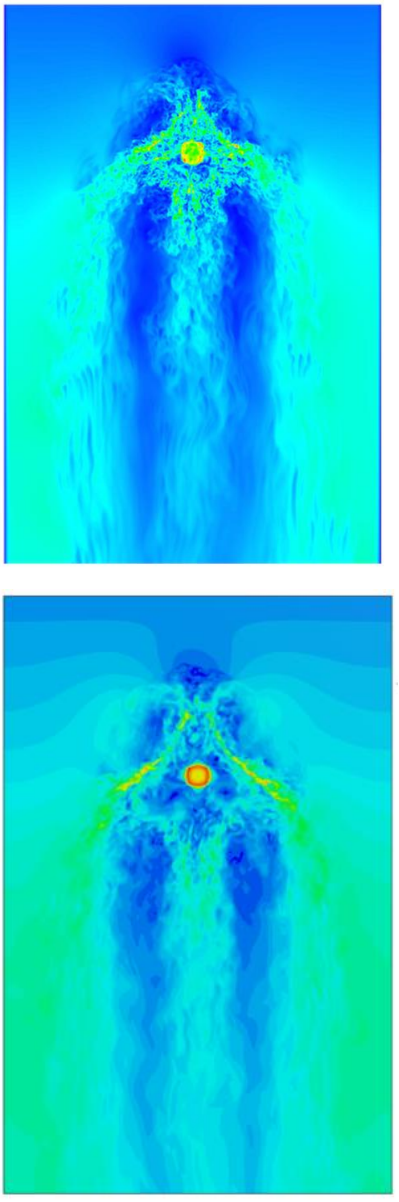

Figure 8. Iso-contours of instantaneous velocity field at the mid cross-section of the downcomer (Left) DNS (Right) LES.

VI. CONCLUSION

In this paper, a simplified pressurized thermal shock scenario of flow impinging the reactor pressure vessel was numerically simulated using the LES turbulence model. This simplified configuration is based on the reference DNS work performed by Shams et al [3]. The flow configuration consists of a cold coolant flowing through a square duct and impinging towards the core barrel wall. Constant fluid properties were considered such that the Prandtl number is a unity, and the Reynold number based on the bulk velocity in the duct is Re=5400. STAR CCM+ code was used to generate a hexahedral mesh of the computational domain and has been used to run the simulation. A second order

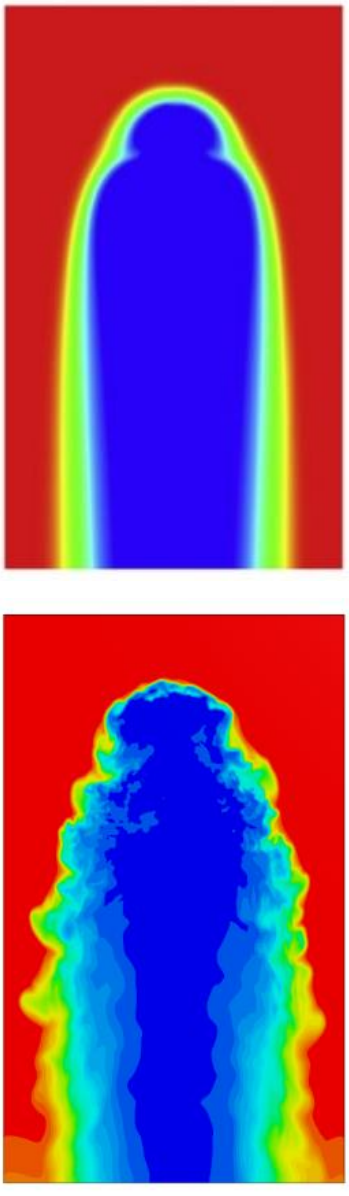

Figure 9 Iso-contour of temperature field (representing the adiabatic boundary condition) (Left) DNS (Right) LES.

central spatial discretization scheme with 5% boundedness was considered, and a second order implicit scheme was used for the temporal discretization.

Preliminary results show similar behaviour to that found in the reference DNS in both the duct and the core barrel. The iso-contours of the velocity fields in the duct show a systematic recirculation region in the whole duct, with special consideration in the corners, indicating a complex nonlinear flow. The velocity field in the duct is in very good agreement to that of the DNS. A qualitative comparison of the obtained LES results is also done with the reference DNS data in the downcomer. In particular, the iso-contours of velocity and temperature fields are compared and has shown good agreement. This also highlights the fact that, if performed properly, LES can also serve as reference to validate low-order turbulence modelling approaches.

Acknowledgments

The authors acknowledge the support provided by King Fahd University of Petroleum and Minerals (KFUPM).

References

[1] IAEA. (2019, February 28). Pressurized thermal shock in nuclear power plants: Good practices for assessment. IAEA. Retrieved November 20, 2022, from https://www.iaea.org/publications/8237/pressurized-thermal-shock-in-nuclear-power-plants-good-practices-for-assessment

[2] Bieder, U., & Rodio, M. G. (2019). Large eddy simulation of the injection of cold ECC water into the cold leg of a pressurized water reactor. Nuclear Engineering and Design, 341, 186–197. https://doi.org/10.1016/j.nucengdes.2018.10.026

[3] A. Shams, D. De Santis, D. Rosa, T. Kwiatkowski, E.J.M. Komen, Direct numerical simulation of flow and heat transfer in a simplified pressurized thermal shock scenario, Int. J. Heat Mass Transf. 135 (2019) 517–540. https://doi.org/10.1016/j.ijheatmasstransfer.2019.01.144.

[4] Wae-hayee, M., Tekasakul, P., Eiamsa-ard, S., & Nuntadusit, C. (2014). Effect of cross-flow velocity on flow and heat transfer characteristics of impinging jet with low jet-to-plate distance. Journal of Mechanical Science and Technology, 28(7), 2909–2917. https://doi.org/10.1007/s12206-014-0534-3

[5] Rundström, D., & Moshfegh, B. (2009). Large-eddy simulation of an impinging jet in a cross-flow on a heated wall-mounted cube. International Journal of Heat and Mass Transfer, 52(3-4), 921–931. https://doi.org/10.1016/j.ijheatmasstransfer.2008.03.035

[6] A. Shams, E.M. Komen, Towards a direct numerical simulation of a simplified pressurized thermal shock, Flow, Turbul. Combust. 101 (2018) 627 – 651.

[7] A. Shams, G. Damiani, D. Rosa, E.M.J. Komen, Design of a single-phase PTS numerical experiment for a reference Direct Numerical Simulation, Nucl. Eng. Des. 300 (2016) 282–296. https://doi.org/10.1016/j.nucengdes.2016.01.038

[8] Shams, A., Roelofs, F., Komen, E. M. J., & Baglietto, E. (2013). Large eddy simulation of a nuclear pebble bed configuration. Nuclear Engineering and Design, 261, 10–19. https://doi.org/10.1016/j.nucengdes.2013.03.040

[9] F. Nicoud and F. Ducros, “Subgrid-Scale Stress Modelling Based on the Square of the Velocity Gradient Tensor,” Flow, Turbulence and Combustion, vol. 62, no. 3, pp. 183–200, 1999, doi: https://doi.org/10.1023/a:1009995426001.